Journal of Thermal Analysis and Calorimetry (2018) 133:1379–1385
https://doi.org/10.1007/s10973-018-7242-7

Hermetic thermal behaviors and specific heat capacities of bis(aminofurazano)furazan and bis(nitrofurazano)furazan

Zhi-Cun Feng[1] · Ming-Yang Du[1] · Lian-Jie Zhai[2] · Kang-Zhen Xu[1] · Ji-Rong Song[1] · Feng-Qi Zhao[2]

Received: 12 September 2017 / Accepted: 4 April 2018 / Published online: 13 April 2018

Abstract
Thermal behaviors of bis(aminofurazano)furazan (BAFF) and bis(nitrofurazano)furazan (BNFF) were studied by the differential scanning calorimetry (DSC) method with a special hermetic high-pressure crucible and compared to that with a common standard Al crucible. The exothermic decomposition processes of the two compounds were completely revealed. The extrapolated onset temperature, peak temperature and enthalpy of exothermic decomposition at the heating rate of 10 °C min^{-1} are 290.2, 313.4 °C and − 2174 J g^{-1} for BAFF, and 265.8, 305.0 °C and − 2351 J g^{-1} for BNFF, respectively. The apparent activation energies of the decomposition process for the two compounds are 115.7 and 131.7 kJ mol^{-1}, respectively. The self-accelerating decomposition temperatures and critical temperatures of thermal explosion are 247.5 and 368.7 °C for BAFF, and 249.6 and 268.1 °C for BAFF, respectively. Both BAFF and BNFF present high thermal stability. The specific heat capacities for the two compounds were determined with the micro-DSC method, and the specific heat capacities and molar heat capacities at 298.15 K are 1.0921 J g^{-1} K^{-1} and 257.9 J mol^{-1} K^{-1} for BAFF, and 1.0419 J g^{-1} K^{-1} and 308.5 J mol^{-1} K^{-1} for BNFF, respectively.

Keywords Furazan · Volatilization · Hermetic thermal behavior · Hermetic crucible · Specific heat capacity

Introduction

1,2,5-Oxadiazole (furazan) is a kind of important heterocyclic compounds [1, 2], and its 2-oxide (furoxan) is also considered as an efficient structural unit of energetic materials because of their positive heat of formation, good thermal stability and high density. If a furazan ring or furoxan ring replaces a nitro group, the density and detonating velocity of a compound can grow about 0.06–0.08 g cm^{-3} and 300 m s^{-1}, respectively [3, 4]. So many multi-furazan ring (furoxan ring) compounds, including chained furazan, macrocyclic furazan and ring-fused furazan compounds, have been reported recently by many researchers [5–16], especially Sheremetev et al., who carried out a lot of research work on this field. Moreover, some derivatives reported have shown good physico-chemical properties and application prospects [17, 18].

Our group also synthesized two chained furazan compounds, bis(aminofurazano)furoxan ($BAFF^O$) and bis(nitrofurazano)furoxan ($BNFF^O$) (ρ_c = 1.937 g cm^{-3}) [19–25], but found that the two compounds have high shock-wave sensitivity coming from the active coordination oxygen atom of the central furoxan ring. Thus, we designed and synthesized bis(aminofurazano)furazan (BAFF) and bis(nitrofurazano)furazan (BNFF) (ρ_c = 1.839 g cm^{-3}) by reduction reaction [26–28]. The relationship between the four compounds is shown in Scheme 1. The synthesis, structure and some denotation properties of BAFF and BNFF have been reported by our group [26]. These compounds have been given good application expectation for their excellent performances.

However, both BAFF and BNFF have strong volatility after melting [28, 29]. In common DSC experiments, the exothermic decomposition processes of the two compounds cannot be observed. Even in the high-pressure DSC experiments, the volatilization of molten sample can only be suppressed partially, and only partial exothermic

✉ Kang-Zhen Xu
xukz@nwu.edu.cn

[1] School of Chemical Engineering, Northwest University, Xi'an 710069, China

[2] Xi'an Modern Chemistry Research Institute, Xi'an 710065, China

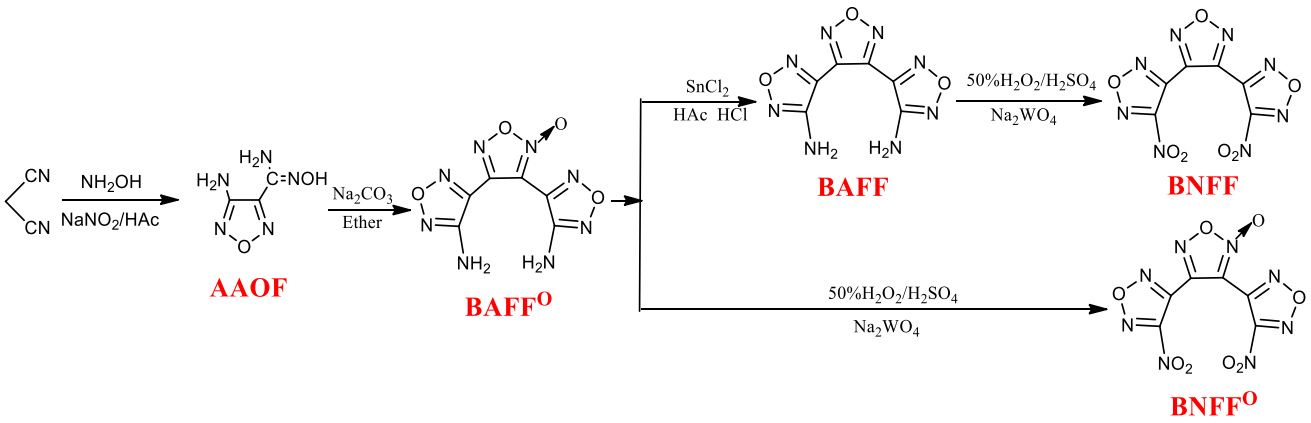

Scheme 1 Relationship between the four multi-furazan ring compounds

decomposition process can be found, so the exothermic decomposition process cannot be characterized perfectly [19, 23]. Because the above-mentioned DSC experiments are all open systems, the volatilization cannot be avoided entirely. Besides, there have been many researchers who studied the thermal transitions of substances in a closed environment to obtain more reliable results [30–32]. Thus, to solve the problem, a special hermetic high-pressure crucible is used necessarily to explore the thermal decomposition of the two compounds.

In this paper, we use a special hermetic crucible to study the thermal behaviors of BAFF and BNFF and determine their specific heat capacities. The results will enhance the understanding on the two compounds for their application.

Materials and methods

Materials

BAFF and BNFF were prepared according to Ref. 26. Their purity is over 99.5% (HPLC).

Methods

DSC experiments were performed using a DSC200F3 apparatus (NETZSCH, Germany) under a nitrogen atmosphere at a flow rate of 100 mL min^{-1}. Two kinds of crucibles were used in experiments. One is a standard common Al crucible, and the other is a special hermetic high-pressure crucible (chrome nickel steel with goldplated surface, max. internal pressure 100 bar, max. temperature 500 °C and Au seals). The heating rates used were 5, 10, 15 and 20 °C min^{-1}, respectively, from ambient temperature to 400 °C. Thermogravimetry/differential thermogravimetry (TG/DTG) experiments were performed using a TG209F3 apparatus (NETZSCH, Germany) under a nitrogen atmosphere at a flow rate of 100 mL min^{-1}, and the crucible used is the standard common Al crucible. The heating rate was 10.0 °C min^{-1} from ambient temperature to 400 °C.

Specific heat capacity was measured with a Micro-DSCIII apparatus (SETARAM, France), using a continuous specific heat capacity model. The standard sample cell with experiment sample was put in apparatus furnace (the mass used for calorimetric measurement was about 200 mg) with the equilibrium time of 1 h, temperature of cooling circulating water bath of 293.15 K, operating temperature range of 283–333 K, temperature accuracy of 10^{-4} K, heat flow accuracy of 10^{-4} mW and heating rate of 0.15 K min^{-1}. The reliability of calorimetry was ensured by determining enthalpy of dissolution of KCl in deionized water at 298.15 K, and the value was 17.264 ± 0.065 kJ mol^{-1} (17.241 ± 0.018 kJ mol^{-1} for the literature value [33]). The obtained equation of specific heat capacity for standard calcined α-Al_2O_3 was C_p (J g^{-1} K^{-1}) = 0.184 + 1.997 × 10^{-3} T (283 K < T < 353 K), and the standard molar heat capacity is 79.44 J mol^{-1} K^{-1} at 298.15 K (79.02 J mol^{-1} K^{-1} for the reference value [34]). All the results indicate that the calorimetric equipment is reliable and accurate.

Results and discussion

Thermal behavior

The DSC curve (**1** in Fig. 1) with common Al crucible indicates that the thermal behavior of BAFF exhibits three stages. The first stage is a melting process, and the extrapolated onset temperature, peak temperature and melting enthalpy at a heating rate of 10 °C min^{-1} are 180.4, 181.6 °C and 119.2 J g^{-1}, respectively. With the

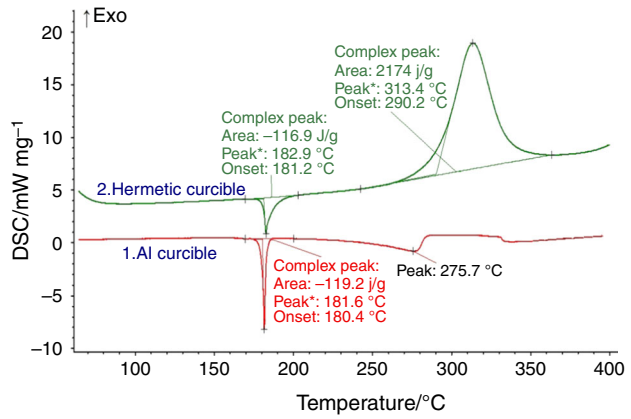

Fig. 1 DSC curves of BAFF at a heating rate of 10 °C min^{-1}

rise of heating temperature, the molten sample begins to slowly volatilize, and the curve presents a slight endothermic trend. At about 275.7 °C, the endothermic process reaches a peak. Then, the thermal behavior exhibits a broad and small exothermic process at the temperature range of 280–335 °C. Heat release of decomposition and heat absorption of volatilization reach a balance at this temperature range. No obvious exothermic decomposition peak of BAFF can be found in DSC curve. Typical TG/DTG curves (Fig. 2) also indicate that BAFF has only one mass-loss process at the temperature range of 150–270 °C. At 268 °C, only 2.6% of mass left, indicating that molten BAFF almost volatilizes entirely. Inevitably, the mass-loss process includes both decomposition and volatilization of the molten BAFF. However, the DSC curve (**2** in Fig. 1) with the special hermetic high-pressure crucible gives a different result. The first process (melting process) is similar to that of common Al crucible. The extrapolated onset temperature, peak temperature and melting enthalpy of it at the heating rate of 10 °C min^{-1} are 181.2, 182.6 °C and 116.9 J g^{-1}, respectively, which are very close to those of common Al crucible despite the fact that there are big differences between these two kinds of crucibles (mass and material quality). However, there is no volatilization of molten BAFF in the special hermetic high-pressure crucible, so no endothermic process can be found after melting. At about 230 °C, the molten BAFF begins to exothermic decomposition, and then, the thermal behavior presents a big and broad exothermic peak at the temperature range of 230–300 °C. The extrapolated onset temperature, peak temperature and decomposition enthalpy of it at the heating rate of 10 °C min^{-1} are 290.2, 313.4.0 °C and − 2174 J g^{-1}, respectively. So the decomposition temperature of BAFF is very high, and the decomposition heat is big. Thus, the thermal stability of BAFF is good in spite of volatilizing after melting.

From the DSC curve (curve **1**) in Fig. 3, the thermal behavior of BNFF has two stages. The first stage is also a melting process, and the extrapolated onset temperature, peak temperature and melting enthalpy at a heating rate of 10 °C min^{-1} are 82.5, 83.9 °C and 69.2 J g^{-1}, respectively. With the rise of heating temperature, the molten BNFF begins to slowly volatilize, and the thermal behavior of BNFF presents a slight endothermic trend. At about 186.4 °C, the endothermic process reaches a peak. No exothermic decomposition peak of BNFF can be found. TG/DTG curves of BNFF in Fig. 4 indicate that there is only one mass-loss process at the temperature range of 75–190 °C. At 230 °C, the molten BNFF almost volatilizes entirely (2.3% at 181 °C). Certainly, the mass-loss process also includes both decomposition and volatilization of the molten BNFF, although no exothermal peak can be found in the DSC curve with the common Al crucible. From the beginning temperature of mass-loss (about 79 °C), we can see that melting and volatilizing are synchronous, but DSC curve (**2** in Fig. 3) with the special high-pressure crucible

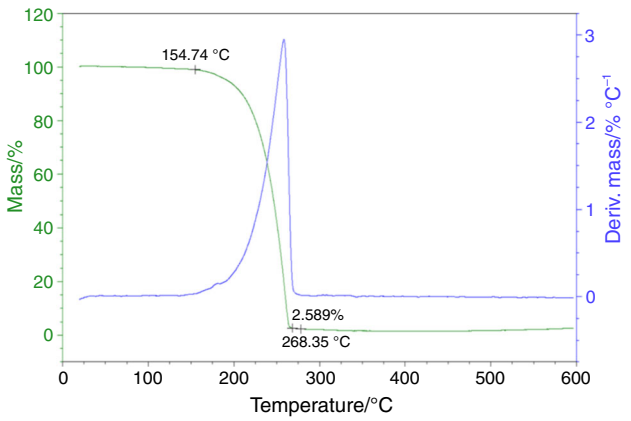

Fig. 2 TG/DTG curves of BAFF at a heating rate of 10 °C min^{-1}

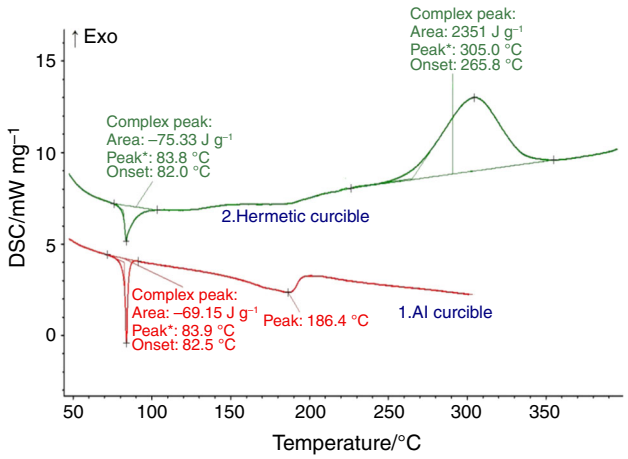

Fig. 3 DSC curves of BNFF a heating rate of 10 °C min^{-1}

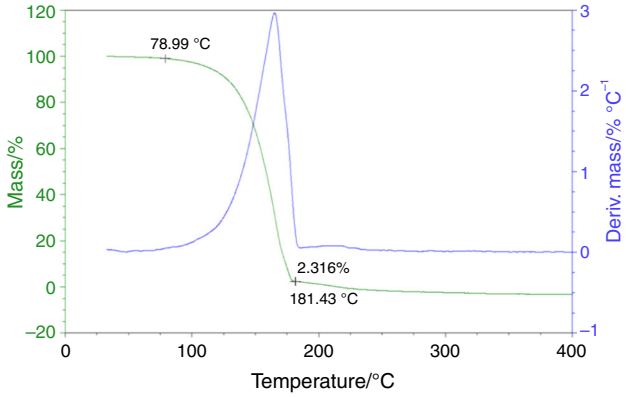

Fig. 4 TG/DTG curves of BNFF a heating rate of 10 °C min^{-1}

indicates that the hermetic thermal behavior of BNFF is much different from that with common Al crucible. The first process (melting process) is similar to that of common Al crucible. The extrapolated onset temperature, peak temperature and melting enthalpy of it at the heating rate of 10 °C min^{-1} are 82.0, 83.8 °C and 75.3 J g^{-1}, respectively, which are consistent with the result of common Al crucible. However, there is no endothermic process after melting. With the rise of heating temperature, the molten BNFF begins to exothermic decomposition, and then, the thermal behavior presents a big and broad exothermic peak at the temperature range of 230–310 °C. The extrapolated onset temperature, peak temperature and decomposition enthalpy of it at the heating rate of 10 °C min^{-1} are 265.8, 305.0 °C and − 2351 J g^{-1}, respectively, so the decomposition temperature of BNFF is also very high and the decomposition heat of it is big. BNFF also presents good thermal stability.

Comparing the hermetic thermal behavior of BNFF with that of BAFF, the melting point decreases greatly from 181.2 to 82.0 °C, after two amino groups changed into two nitro groups in molecule. As casting explosive, it is very beneficial. Moreover, the decomposition temperature reduces from 290.2 to 265.8 °C, but the decomposition heat rises slightly (2174–2351 J g^{-1}).

Apparent activation energy

The kinetic parameters [the apparent activation energy (E) and pre-exponential constant (A)] of the exothermic decomposition process were studied with a multiple heating method. The extrapolated onset temperature (T_e) and peak temperature (T_p) at the different heating rates for BAFF and BNFF are listed in Table 1. The calculated values of kinetic parameters by Kissinger method and Ozawa method [35, 36] are also listed in Table 1. The apparent activation energy obtained by Kissinger method is all consistent with that by Ozawa method for the two compounds. The linear correlation coefficients (r) are all close to 1. Thus, the results are credible. Moreover, the apparent activation energy of the decomposition process for the two compounds is very low, indicating that molten BAFF and BNFF easily decompose at high temperature.

The self-accelerating decomposition temperature (T_{SADT}) and critical temperature of thermal explosion (T_b), which can be obtained by Eqs. (1) and (2) [37–39], are two important parameters required to ensure safe storage and process operations for energetic materials and then to evaluate the thermal stability. T_{SADT} and T_b are 247.5 and 368.7 °C for BAFF, and 249.6 and 268.1 °C for BNFF, respectively, also indicating that both BAFF and BNFF have high thermal stability.

$$T_{SADT} = T_{e0} = T_{ei} - n\beta_i - m\beta_i^2 \quad i = 1 - 4 \tag{1}$$

$$T_b = \frac{E_O - \sqrt{E_O^2 - 4E_O R T_{e0}}}{2R} \tag{2}$$

where β is the heating rate and E_O is the apparent activation energy obtained by Ozawa method.

Specific heat capacity

The continuous specific heat capacities of the two compounds were measured successively, and the determination results are shown in Figs. 5 and 6. We can see that specific heat capacity for BAFF presents a linear relationship with temperature in the determining temperature range, but specific heat capacity for BNFF increases greatly after 305 K and presents a cubic relationship with temperature. The reason for the abnormal result should be that BNFF has a low melting point (83.5 °C) and a relatively wide melting range (DSC curve in Fig. 3). BNFF begins to change at a very low temperature, and the change is unobservable in common DSC result. However, the change is very obvious in micro-DSC curve (Fig. 6). Meanwhile, the values of specific heat capacity come from the theoretical Eq. (3):

$$C_p = \frac{A_s - A_b}{m_s \times \beta} \tag{3}$$

where C_p is the specific heat capacity, A_s and A_b are the heat flows of the sample and blank, m_s is the amount of the sample and β is the heating rate.

Thus, the small change of heat flow will affect the specific heat capacity result greatly. Fitted specific heat capacity equations for BAFF and BNFF are as follows:

Table 1 The values of T_e, T_p and kinetic parameters of decomposition process for BAFF and BNFF

Sample	Heating rate/K min^{-1}	T_e/°C	T_p/°C	E_k/kJ mol^{-1}	log(A/s^{-1})	r_k	E_o/kJ mol^{-1}	r_o
BAFF	5.0	270.2	296.0	115.7	8.16	0.9968	119.3	0.9972
	10.0	290.2	313.4					
	15.0	296.2	320.9					
	20.0	303.3	327.4					
BNFF	5.0	256.1	295.3	131.7	9.75	0.9847	134.4	0.9868
	10.0	265.8	305.0					
	15.0	269.1	314.0					
	20.0	278.8	322.8					

Subscript k, data obtained by Kissinger method; subscript o, data obtained by Ozawa method

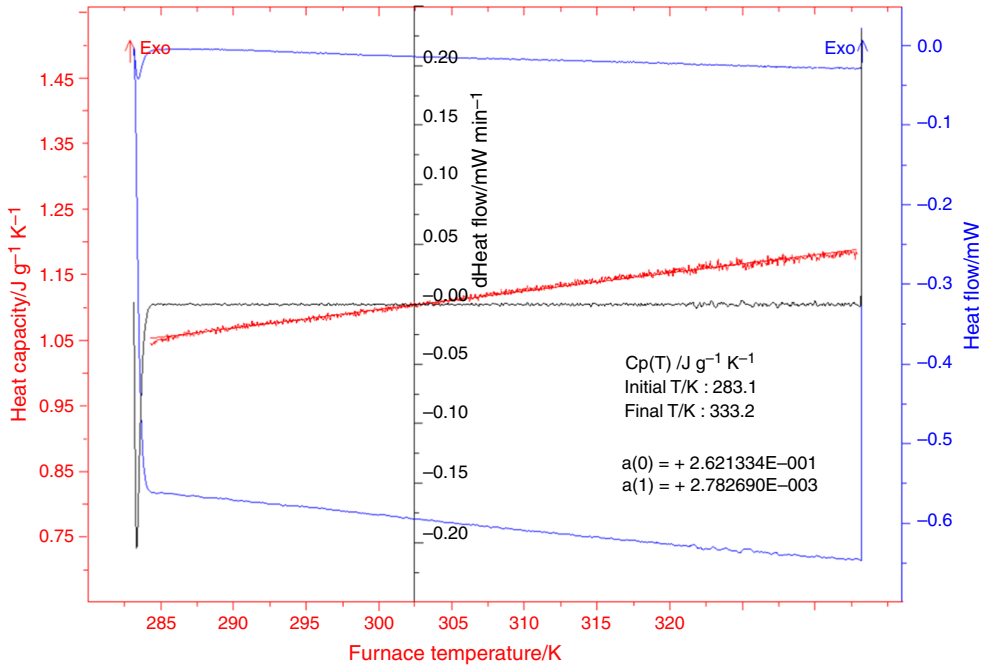

Fig. 5 Determination results of the continuous specific heat capacity of BAFF

$$C_p(\text{BAFF, J g}^{-1}\text{ K}^{-1}) = 0.2621 + 2.7827 \times 10^{-3}T \times (R^2 = 0.9986,\ 285\text{ K} < T < 330\text{ K}) \quad (4)$$

$$C_p(\text{BNFF, J g}^{-1}\text{ K}^{-1}) = -1.7416 \times 10^2 + 1.7631T - 5.9240 \times 10^{-3}T^2 + 6.6468 \times 10^{-6}T^3 (R^2 = 0.9945,\ 285\text{ K} < T < 330\text{ K}) \quad (5)$$

If reducing the temperature range (285–303 °C), the specific heat capacity for BNFF can also be fitted to linear equation as:

$$C_p(\text{BNFF, J g}^{-1}\text{K}^{-1}) = 0.0876 + 3.2008 \times 10^{-3}T \times (R^2 = 0.9874,\ 285\text{ K} < T < 303\text{ K}) \quad (6)$$

The specific heat capacity and molar heat capacity at 298.15 K are 1.0921 J g^{-1} K^{-1} and 257.9 J mol^{-1} K^{-1} for BAFF, and 1.0419 J g^{-1} K^{-1} and 308.5 J mol^{-1} K^{-1} for BNFF, respectively. The specific heat capacity of BAFF is greater than that of BNFF, indicating that amino group can make a greater contribution to the specific heat capacity than nitro group.

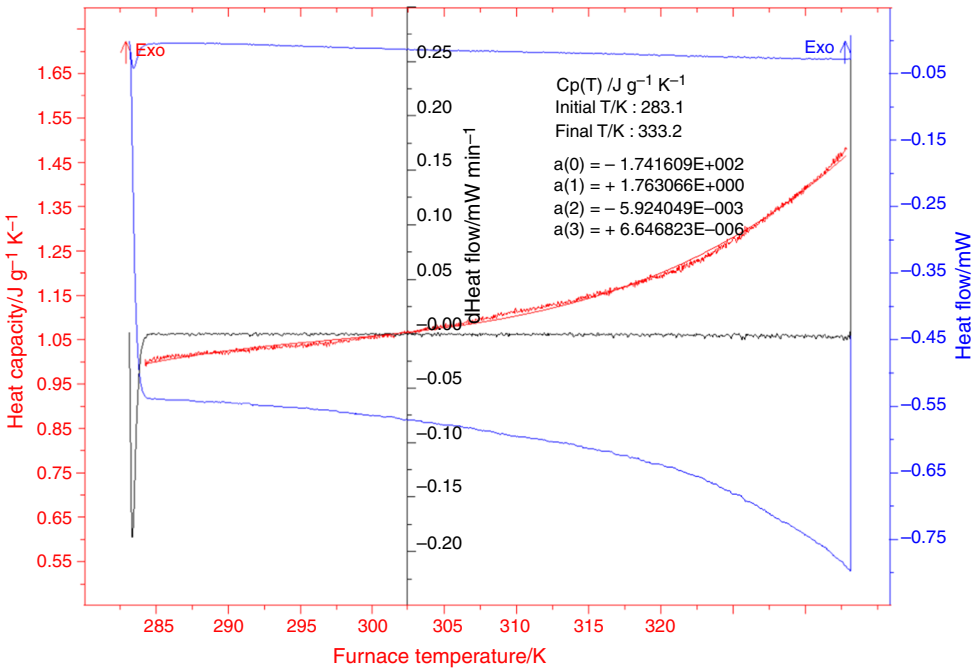

Fig. 6 Determination results of the continuous specific heat capacity of BNFF

Conclusions

In summary, we used a special hermetic high-pressure crucible to study the thermal behaviors of two energetic materials on account of their volatility after melting. The exothermic decomposition processes for the two compounds are completely revealed. Hermetic thermal behaviors of both bis(aminofurazano)furazan (BAFF) and bis(nitrofurazano)furazan (BNFF) present a melting process and a big and broad exothermic decomposition process. The study results indicate that BAFF and BNFF all possess high thermal stability. The specific heat capacity equation and molar heat capacity at 298.15 K for the two compounds were obtained. The specific heat capacity of BAFF is greater than that of BNFF, indicating that amino group can make a greater contribution to specific heat capacity than nitro group.

Acknowledgements This work was supported by the National Natural Science Foundation of China (21673178).

References

1. Kinney R, Harwood HJ. The structure of furazan oxides. J Am Chem Soc. 1927;49:514–6.
2. Olofson RA, Michelman JS. Furazan. J Org Chem. 1965;30:1854–6.
3. Li ZX, Tang SQ. Review on the synthesis of furoxan derivatives. Chin J Energy Mater. 2006;14(1):77–9.
4. Huang M, Li HZ, Huang YG, Dong HS. Synthesis of diaminoazofurazan and diaminoazoxyfurazan. Energy Mater. 2004;12:91–4.
5. Sheremetev AB. Chemistry of furazans fused to five-membered rings. J Heterocycl Chem. 1995;32:371–5.
6. Sheremetev AB, Kulgina VO, Aleksandrova NS, Dmitriev DE, Strelenko YA, Lebedev VP, Matyushin YN. Dinitro trifurazans with oxy, azo, and azoxy bridges. Propellant Explos Pyrotech. 1998;23:142–8.
7. Ivanova OA, Averina EB, Kuznetsova TS, Zefirov NS. Synthesis of new 3,4-disubstituted furazans. Chem Heterocycl Commun. 2000;36:1091–6.
8. Sheremetev AB, Mantseva EV, Dmitriev DE, Sirovskii FS. Transetherification of difurazanyl ethers as a route to unsymmetrical derivatives of difurazanyl ether. Russ Chem Bull. 2002;111:659–62.
9. Talawar MB, Sivabalan R, Senthilkumar N, Prabhu G, Asthana SN. Synthesis characterization and thermal studies on furazan and tetrazine-based high energy materials. J Hazard Mater. 2004;113:11–5.
10. Sheremetev AB, Shamshina YL, Dmitriev DE. Synthesis of 3-alkyl-4-aminofurazans. Russ Chem Bull. 2005;54:1032–6.
11. Sheremetev AB, Palysaeva NV, Struchkova MI. The first synthesis of 3-nitro-4-((s-tetrazin-3-yl)amino)furazans. Mendeleev Commun. 2010;20:350–3.
12. Chavez D, Klapötke TM, Parrish D, Piercey D, Stierstorfer GJ. The synthesis and energetic properties of 3,4-bis(2,2,2-trinitroethylamino)furazan (BTNEDAF). Propellant Explos Pyrotech. 2014;39:641–8.
13. Sheremetev AB, Lyalin BV, Kozeev AM, Palysaeva NV, Struchkova MI, Suponitsky KY. A practical anodic oxidation of aminofurazans to azofurazans: an environmentally friendly Route. RSC Adv. 2015;47:37617–9.
14. Makhova NN, Ovchinnikov IV, Kulikov AS, Khakimov DV, Molchanova MS, Pivina TS. Diaminofuroxan: synthetic approaches and computer-aided study of thermodynamic stability. Propellant Explos Pyrotech. 2012;37:549–57.
15. Sheremetev AB, Kulagina VO, Ivanova EA. Zero-hydrogen furazan macrocycles with oxy and azo bridges. J Org Chem. 1996;61:1510–2.
16. Zelenin AK, Trudell ML, Gilardi RD. Synthesis and structure of dinitroazofurazan. J Heterocycl Chem. 1998;35:151–5.

17. Pagoria PF. A review of energy materials synthesis. Thermochim Acta. 2002;384:187–8.
18. Sikder AK, Sikder NA. Review of advanced high performance, insensitive and thermally stable energetic materials emerging for military and space applications. J Hazard Mater. 2004;112:1–15.
19. Zheng W, Wang JN. Review on 3,4-bisnitrofurazanfruoxan (DNTF). Chin J Energy Mater. 2006;14(6):463–4 **(in Chinese)**.
20. Hu HX, Zhang ZZ, Zhao FQ, Xiao C, Wang QH, Yuan BH. A study on the properties and application of high energy density material 3,4-bisnitrofurazanfruoxan. Acta Amamentarii. 2004;25(2):155–8.
21. Zhou YS, Zhang ZZ, Li JK, Guan XR, Huang XP, Zhou C. Crystal structure of 3,4-bisnitrofurazanfruoxan. Chin J Explos Propell. 2005;28(2):43–4.
22. Wang QH. Properties of DNTF-base melting cast explosives. Chin J Explos Propell. 2003;26(3):57–9.
23. Zhao FQ, Chen P, Hu RZ. Thermochemical properties and non-isothermal decomposition reaction kinetics of 3,4-bisnitrofurazanfruoxan. J Hazard Mater. 2004;113:67–71.
24. Zhao FQ, Chen P, Luo Y. Study on the composite modified double base propellant containing 3,4-bisnitrofurazanfruoxan. J Propuls Technol. 2004;26(6):570–3.
25. Wang J, Dong HS, Huang YG, Li JS. Studies on the preparation and crystal structure of 3,4-diaminofurazanfruoxan. Acta Chim Sin. 2006;64(2):158–62.
26. Zhang Y, Zhou C, Wang BZ, Zhou YS, Xu KZ, Jia SY, Zhao FQ. Synthesis and characteristics of bis(nitrofurazano)furazan (BNFF), an insensitive material with high energy-density. Propellant Explos Pyrotech. 2014;39:809–14.
27. Wang XJ, Xu KZ, Sun Q, Wang BZ, Zhou C, Zhao FQ. The insensitive energetic material trifurazano-oxacycloheptatriene (TFO): synthesis and detonation properties. Propellant Explos Pyrotech. 2014;40:9–12.
28. Kim TK, Choe JH, Lee BW, Chung KH. Synthesis and characterization of BNFF analogues. Bull Korean Chem Soc. 2012;33:2765–8.
29. Zhao K, Wang HX, Jiang QL, Liu RP. The research on volatility of 3,4-bisnitrofurazanfruoxan. Sci Tech Eng. 2014;14(29):271–3.
30. Mukherjee I, Rosolen M. Thermal transitions of gelatin evaluated using DSC sample pans of various seal integrities. J Therm Anal Calorim. 2013;114:1161–6.
31. Zhong Y, Li X, Gu Z, Wang X, Yang L, Yang X, Zhang Z, Zhong B. Thermal studies on Li(CH3CN)4PF6 and Li(C4H10O2)2PF6 complexes by the TG–DTA–MS and DSC. J Therm Anal Calorim. 2018;131:1287–93.
32. Muñoz-Sánchez B, Nieto-Maestre J, Imbuluzqueta G, MarañónIñigo I, Iparraguirre-Torres I, García-Romero A. A precise method to measure the specific heat of solar salt-based nanofluids. J Therm Anal Calorim. 2017;129:905–10.
33. Zhang Y, Wu H, Xu KZ, Zhang WT, Song JR, Zhao FQ, Hu RZ. Thermolysis, non-isothermal decomposition kinetics, specific heat capacity and adiabatic time-to-explosion of $(Cu(NH_3)_4)(DNANT)_2$ [DNANT = Dinitroacetonitrile). J Phys Chem A. 2014;118:1168–74.
34. Ditmars DA, Ishihara S, Chang SS, Bernstein G, West ED. Enthalpy and heat-capacity standard reference material: synthetic sapphire (alpha-Al_2O_3) from 10 to 2250 K. J Res Natl Bur Stand. 1982;87(2):159–63.
35. Kissinger HE. Reaction kinetics in differential thermal analysis. Anal Chem. 1957;29:1702–5.
36. Ozawa TA. Method of analyzing thermogravimetric data. Bull Chem Soc Jpn. 1965;38:1881–6.
37. Zhang TL, Hu RZ, Xie Y, Li FP. The estimation of critical temperatures of thermal explosion for energetic materials using non-isothermal DSC. Thermochim Acta. 1994;244:171–6.
38. Hu RZ, Gao SL, Zhao FQ, Shi QZ, Zhang TL, Zhang JJ. Thermal analysis kinetics. 2nd ed. Beijing: Science Press; 2008 **(in Chinese)**.
39. Xu KZ, Song JR, Zhao FQ, Ma HX, Gao HX, Chang CR, Ren YH, Hu RZ. Thermal behavior, specific heat capacity and adiabatic time-to-explosion of G(FOX-7). J Hazard Mater. 2008;158:333–7.